EAST EUROPEAN JOURNAL OF PHYSICS. 2. 353-357 (2024)
DOI:10.26565/2312-4334-2024-2-42 ISSN 2312-4334

STRUCTURAL FEATURES OF SILICON WITH TIN IMPURITY

Sharifa B. Utamuradova, Bakhodir B. Bokiyev, Dilorom S. Pulatova
Institute of Semiconductor Physics and Microelectronics at the National University of Uzbekistan, Tashkent, Uzbekistan
**Corresponding Author e-mail: boqiyevb@gmail.com*
Received April 1, 2024; revised April 22, 2024; accepted May 10, 2024

In this work, samples of single-crystalline silicon doped with tin were studied using X-ray diffraction and electron microscopy. It has been established that at a scattering angle of $2\theta \approx 36.6°$ in the X-ray diffraction patterns of n-Si and Si<Sn> samples, structural reflections (110) of the corresponding SiO_2 nanocrystallites with lattice parameters $a = b = 0{,}4936$ нм и c = 0,5212 nm and c = 0.5212 nm, belonging to the hexagonal crystal lattice and space group $P3_21$. The formation of tin nanocrystallites with sizes of 9.1 and 8 nm in the near-surface regions of the Si<Sn> matrix crystal lattice was discovered.
Keywords: *Silicon; Tin; X-ray diffraction; Subcrystallite crystal lattice; Nanocrystallite*
PACS: 61.72. Ff, 61.72.Qq

INTRODUCTION

As is known, a number of physical properties of semiconductor materials can change as a result of doping with various doping atoms [1-4]. In this case, it is important that the input atoms are evenly distributed throughout the volume. But with traditional doping methods, in particular, in the process of growing bulk single crystals, it is difficult to control a sufficient distribution of input atoms over the volume. This is why it is especially relevant to study how the input atoms are arranged in the crystal structure [5,6]. In addition, it is known that the degree of mono- and polycrystallinity of the silicon structure depends on the impurity composition, the perfection of the defect structure, the distribution of impurities and the lattice mismatch parameters of the matrix and alloying elements [7-10].

In connection with this, the purpose of this work was to study various structural parameters of Si doped with tin atoms using modern methods of X-ray diffraction studies.

EXPERIMENTAL TECHNIQUE

The initial material was samples in the form of wafers made of single-crystalline n-type silicon with a resistivity of 40 Ω·cm, grown by the Czochralski method. The main disadvantages of growing single-crystal silicon using the Czochralski method include the increased content in the resulting crystals of background impurities of oxygen and carbon atoms with concentrations of up to $2 \cdot 10^{18}$ cm^{-3} and up to $5 \cdot 10^{16}$ cm^{-3}, respectively. Among background impurities, the problem of the presence of oxygen atoms in silicon has remained very relevant for many years [11-14].

Doping silicon with tin atoms was carried out by diffusion from the gas phase at a temperature of 1100°C in quartz ampoules under a vacuum of 1 mTorr for 2 hours, followed by rapid cooling.

The structural and phase states of the samples under study were monitored using an Empyrean Malvern X-ray diffractometer. The OriginPro2019 program was used to determine the peak maximum. X-ray diffraction measurements were carried out in the Bragg–Brentano beam geometry in the scattering angle range $2\theta_b$ = from 10° to 90° continuously at a scanning speed of 0.33 degrees/min with an angular step of 0.0200 (deg).

RESULTS AND DISCUSSION

In Figure 1a shows the X-ray diffraction pattern of the n-Si sample (ρ=40 Ω·cm), from which it follows that at small scattering angles (in the range $2\theta = 12° \div 20°$) there is a wide and low-intensity diffuse reflection on the X-ray pattern, as well as above the level of inelastic background, structural reflections with different intensities are observed. Typically, low-intensity diffuse reflection is due to the presence on the surface of n-Si samples of amorphous clusters with dimensions of 1÷1.5 nm, consisting of silicon oxide [8]. The silicon oxide layer on the surface of silicon samples reforms over time, so the amorphous layer is usually removed by chemical etching before the process of doping impurity atoms [15].

In the given X-ray diffraction patterns at scattering angles of $2\theta = 28{,}52°$ with d/n = 0.3138 nm and $2\theta = 95{,}2°$ with d/n = 0.1045 nm (n is the serial number of the plane and d is the interplanar distance) there are two structural reflections from lines of a selective nature with a main (111)Si peak with high intensity and a (333)Si peak with weak intensity, respectively. The structure line (333) is the third order of the high-intensity reflection (111). At a scattering angle of $2\theta = 25.68°$, the β reflection component (111) is observed. Analysis of the above structural results showed that the surface of the n-Si sample wafers corresponds to the (111) crystallographic orientation.

Splitting of the structural reflection (111) into α_1 and α_2 components, having the values $I(\alpha_1) = 2I(\alpha_2)$, as well as its half-width (FWHM = $4.1 \cdot 10^{-3}$ rad) and high intensity ($3 \cdot 10^4$ imp·sec^{-1}) indicates a high degree of perfection of the lattice of n-Si silicon samples (Fig. 2a).

Cite as: Sh.B. Utamuradova, B.B. Bokiyev, D.S. Pulatova, East Eur. J. Phys. 2, 353 (2024), https://doi.org/10.26565/2312-4334-2024-2-42
© Sh.B. Utamuradova, B.B. Bokiyev, D.S. Pulatova, 2024; CC BY 4.0 license

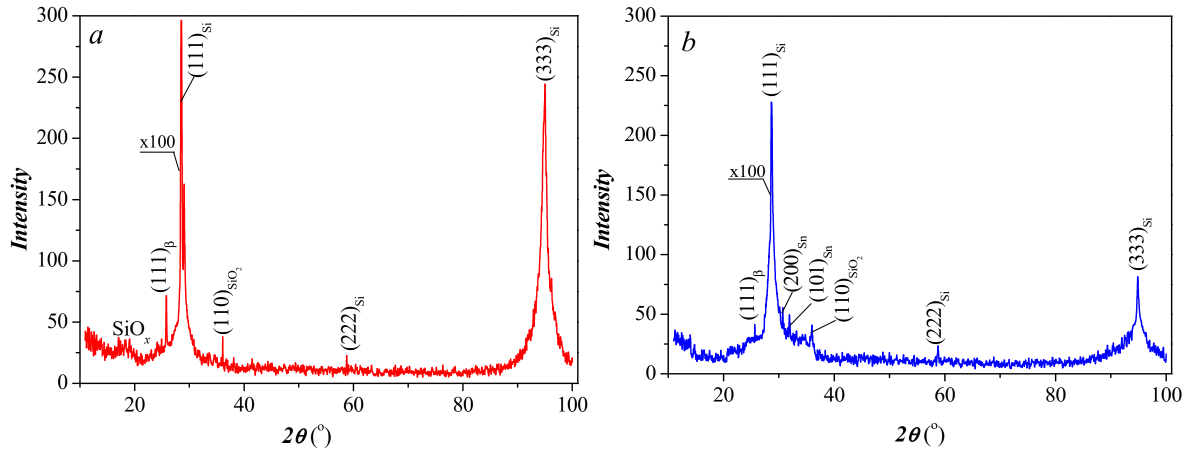

Figure 1. X-ray diffraction patterns of n-Si (a) and Si<Sn> (b) samples

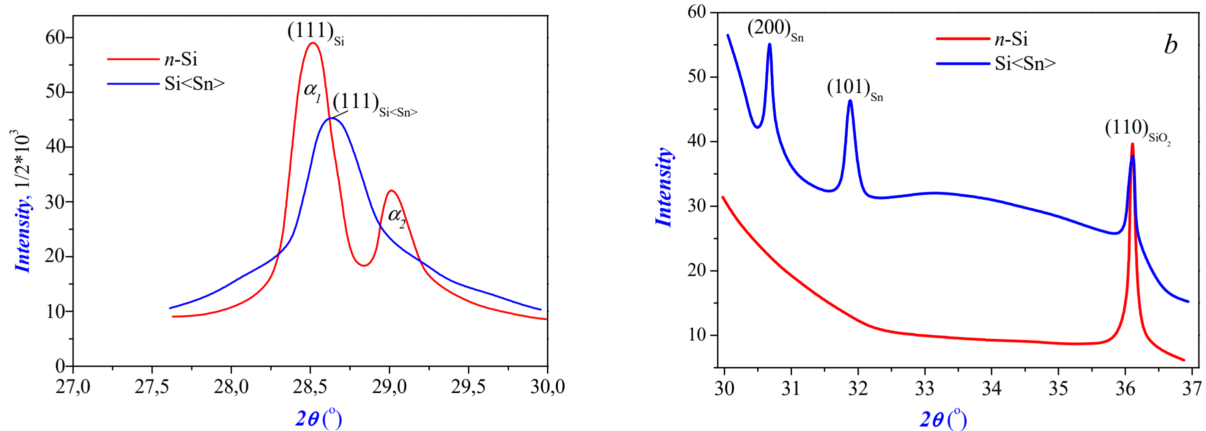

Figure 2. Shapes of the main (111) selective reflections (a), as well as structural (200), (101) and (110) lines (b) on the X-ray diffraction pattern of n-Si and Si<Sn> samples

From the experimental data of the main reflection (111), it was determined that the average size (L) of subcrystallites (blocks) in n-Si samples is determined by the Selyakov–Scherrer formula:

$$L=K\cdot\lambda/\beta\cdot\mathrm{Cos}\theta, \quad (1)$$

where K is the dimensionless particle shape factor (Scherrer constant, which is equal to 0.94), λ is the x-ray wavelength (0.154 nm), β is the reflection width (111) at half maximum (in radians) and θ is the diffraction angle (Bragg angle), and the average size L = 6.5 nm.

Also, the lattice parameter of blocks in n-Si samples was determined from (111) reflections using the extrapolated Nelson-Riley function (x) [15]

$$x = 1/2(\mathrm{Cos}^2\theta/\mathrm{Sin}\theta+\mathrm{Cos}^2\theta/\theta), \quad (2)$$

using the following relationship:

$$y = kx + b, \quad (3)$$

where y is the lattice parameter, k is the slope of the linear trend. When extrapolating $x\to 0$ ($\theta = 90°$), the value y = b corresponds to the “true” value of the lattice parameter, the value of which is 0.5439 nm.

In addition, at a scattering angle of $2\theta = 58.68°$ with d/n = 0.1546 nm, the X-ray diffraction pattern of the n-Si sample contains the second (222) Si order of the main structural line (111). In [16], the reason for the appearance of diffraction reflection (222) in an X-ray diffraction pattern in a distorted lattice of single-crystal silicon was reported, and this reflection is a forbidden reflection according to the selection rules. The value is determined to be $15\cdot 10^{-4}$ using the ratio I(222)/I(111) and this value is partially greater than 10^{-4}. This indicates the appearance of an unsaturated bond under a nonuniformly distributed oxygen atom in the silicon lattice. Additional confirmation of the presence of inclusions of oxygen atoms in the silicon lattice is provided by the SiO_x (amorphous) and SiO_2 (crystalline) forms formed in locally and defect-prone regions of the n-Si crystal lattice. Diffuse reflection related to the SiO_x form is caused by amorphous phases of silicon oxide [17], and diffraction reflection (110) related to the SiO_2 form is observed at a scattering angle of $2\theta \approx 36.6°$ (with $d/n \approx 0.247$ nm) of the X-ray diffraction pattern. This indicates the formation of SiO_2 nanocrystallites at the interfaces between blocks in n-Si samples. The average size of these nanocrystallites was experimentally determined

by formula (1), which is 17 nm. The lattice parameter of quartz nanocrystalites at room temperature was also determined from the analysis of experimental results of (110) reflection using the expressions [18]:

$$\frac{1}{d^2(hkl)} = \frac{4}{3}\left[\frac{h^2+hk+k^2}{a^2}\right] + \frac{l^2}{c^2}, \quad (4)$$

$$and\ c = \frac{\lambda}{sin\theta}. \quad (5)$$

Here, taking into account h = 1, k = 1 and l = 0 from reflection (110), the last term of expression (4) is equal to zero, and from this expression a and b are determined by the following relation:

$$a = b = 2d\sqrt{\frac{1}{3}(h^2 + hk + k^2)}. \quad (6)$$

The lattice parameters are a = b = 0.4936 nm and c = 0.5212 nm, respectively, which in turn showed that the unit cell of these nanocrystalites belongs to the hexagonal crystal lattice and space group $P3_21$. Knowing the matrix lattice parameters of silicon and quartz nanocrystalites, it is possible to determine their specific volume, which differs by almost 23%. This, in turn, indicates that the elastic energy associated with structural defects arising at the local boundaries of silicon crystal matrix lattices as a result of the inhomogeneous distribution of oxygen is spent on the formation of nanocrystalites at the interfaces between blocks of n-Si samples. Therefore, a forbidden diffraction reflection of the second order (222) appeared in the X-ray diffraction patterns of n-Si samples under the influence of this process [16]. Low-intensity (222) reflection indicates the presence of minor local defects in the matrix lattices surrounding the formed nanocrystalites. If these nanocrystalites are not formed at the interfaces of blocks of n-Si samples, then in the diffraction pattern there is an expansion of the main structural line (111) and an increase in the second-order structural line (222), as well as defects leading to a change in the level of the inelastic background of the X-ray diffraction pattern, would be formed in the matrix lattice [19].

In Fig. 1-a and Fig. 1-b shows X-ray diffraction patterns of n-Si and Si<Sn> samples, which are very different from each other. Analysis and comparison of these drawings show that the intensity of the main reflection (111) in Si<Sn> samples at a scattering angle of $2\theta = 28.63^\circ$with d/n = 0.3144 nm decreased by 2 times and shifted towards larger angles ($\Delta\theta = 0.11°$), also the appearance of its β-component was observed at a scattering angle of $2\theta = 25.75^\circ$, respectively. This, in turn, indicates that due to the fact that silicon and tin are isovalent atoms, they are partially interchangeable in the matrix lattice of Si<Sn> samples, since the X-ray scattering intensity is proportional to the atomic number (Z) of the constituent elements [18].

The sufficiently maximum intensity and half-width (FWHM = 9.6 10^{-3}rad) of the main reflection (111) means that the Si<Sn> samples have a fairly perfect crystal structure and the direction of the surface of these samples corresponds to the crystallographic orientation (111). From the experimental data of the main reflection (111), it was determined that the lattice parameter of the blocks in the Si<Sn> samples according to formulas (2) and (3), which is equal to $a_{Si<Sn>}$ = 0.5435 nm. The mismatch of the crystal lattice parameters of the blocks in the n-Si and Si<Sn> samples was 0.00037 when determined using the following expression [20]:

$$\xi = 2\frac{a_{Si} - a_{Si<Sn>}}{a_{Si} + a_{Si<Sn>}}. \quad (7)$$

The average block size in Si<Sn> samples, estimated by formula (1) from the experimental results of this reflection, was 29.9 nm. However, although this structural reflex shifts towards larger angles and exhibits its asymmetry, it is not completely separated into its component α_1 and α_2 emissions (Fig. 2-b). This indicates that, as the authors of [21] note, elastic microdistortions of a growth nature arise during the diffusion of impurity atoms into the silicon crystal lattice in the temperature range 800ºC ÷ 1200ºC. As we noted above, due to the formation of such microdamages in the crystal lattice of Si<Sn> samples, a forbidden second-order reflection of the (222)Si main reflection is observed in the X-ray diffraction pattern at a scattering angle of $2\theta = 58.75^\circ$ with d/n = 0.1570 nm. In addition, the ratio I(222)/I(111) of I(111) intensity to I(222) intensity is 7.8×10^{-4} and this value is 2 times less than the value determined for n-Si samples. This, in turn, indicates that the number of oxygen accumulations in tin-doped silicon samples is two times less than the number of accumulations in the crystalline form of n-Si samples.

In addition, due to the chemical treatment to remove the oxide layer from the n-Si surface before doping with tin atoms, which have the amorphous properties of silicon oxide, no diffusion reflection was observed in the X-ray diffraction patterns of the Si<Sn> samples. However, the authors of [17] showed that oxygen atoms do not have a large effect on the distortion of the silicon crystal lattice, but on the contrary, the formation of localized microdistortions in the silicon crystal lattice occurs due to the difference in the ionic radii of silicon (0.42 nm) and tin (0 .71 nm), located at the nodes. Note that in Fig. 2-a and 2-b, on the right side of the main reflection, a diffusion slope was observed, which, in turn, indicates the formation of stacking faults in the silicon crystal lattice, which are often encountered in many cases. In most cases, due to the difference between the covalent radius of a tin atom (RSn = 1.40Å) and the covalent radius of a silicon atom (RSi=1.14Å), they prefer to be located at nodes at the interfaces of silicon subcrystallites [23]. This, in turn, allows the

formation of new types of small tin nanocrystals of various sizes and crystallographic orientations in these places, preventing the occurrence of a large number of microdistortions in the silicon crystal lattice [24].

In addition, three more structure lines are observed above this diffusion reflection of the X-ray diffraction pattern at scattering angles of $2\theta = 30.67^{\circ}$, $2\theta = 31.84^{\circ}$ и $2\theta = 36.57^{\circ}$ nm, respectively (see Fig. 2-a and 2-b). These structure lines are caused by tin nanocrystallite phases with crystallographic orientation (200) and (101) between the d/n = 0.2948 nm and d/n = 0.2814 nm planes. Also, a narrower (1.58×10^{-2}rad) reflection (110) with d/n = 0.2469 nm, which belonged to silicon dioxide nanocrystallites with an average size of 14 nm. From these half-width values (1.65×10^{-2} rad) and (1.88×10^{-2} rad) (200) and (101) reflections, it was determined that the average sizes of these tin nanocrystallites, calculated by formula (1), were 9.1 nm and 8 nm respectively. This, in turn, indicates that the formation of tin nanocrystallites in the (101) and (200) crystallographic planes occur under the influence of the oriented matrix lattice of Si<Sn> (111) samples. This case leads to an increase in the consistency between tin nanocrystallites and silicon matrix lattices, as well as to an increase in the hardness of samples based on them [22].

In addition, tin nanocrystallites with sizes of 9.1 and 8 nm, formed on the matrix lattice of Si<Sn> samples, can exhibit quantum-size effects, which are of great interest in modern nanotechnologies. Therefore, using the expression

$$\lambda_D = \frac{1}{e}\sqrt{\frac{\varepsilon\varepsilon_0 kT}{n}}. \tag{8}$$

The value of the Debye length (λ_D) of screening for the samples under study was calculated, which is equal to 13.2 nm. Here, ε is the relative dielectric constant of Si<Sn> samples (ε = 11.7), ε_0 is the dielectric constant, k is Boltzmann's constant, T is temperature, e is the electron charge, n is the concentration of current carriers, in this case equal to 10^{17} cm^{-3}. The average size of tin nanocrystallites determined from experimental data is less than the Debye electron length.

Thus, we can conclude that tin atoms partially (in low concentrations) exchange places with silicon atoms, and the rest combine in the near-surface regions of the Si<Sn> samples, forming tin nanocrystallites. If tin atoms were replaced by homogeneous silicon atoms in the matrix crystal lattice, then the intensity of the main (111) and its third order (333) reflections should increase. However, in the X-ray diffraction patterns of Si<Sn> samples, a decrease in the intensity of structural reflections (111) and (333), as well as reflections related to tin nanocrystallites in other crystallographic orientations, was observed. This, in turn, indicates that tin atoms accumulate in defective regions of the silicon crystal lattice. Since in these regions of the lattice there is no saturation of the chemical bonds of the constituent atoms, they are considered high-potential nodes and are formed at the boundary sections of blocks belonging to the category of near-surface sections. The authors of the study [25] predicted that since the rate of diffusion of tin atoms through the surfaces and border regions of silicon is twice the rate of bulk diffusion, the penetrating atoms will easily move and accumulate in defective regions of the matrix lattice. Such diffusion processes cause the rapid formation of tin nanocrystallites in defective regions and block interfaces in Si<Sn> samples. The formation of such nanocrystallites at block boundaries in silicon samples may also be due to the fact that $E_{Sn-Sn}>E_{Si-Sn}$ и $E_{Sn-Sn}>E_{Si-Si}$.

$$\frac{1}{d^2(hkl)} = \frac{h^2+k^2}{a^2} + \frac{l^2}{c^2}, \tag{9}$$

$$and\ c = \frac{1}{\sqrt{3}}\frac{\lambda}{sin\theta}. \tag{10}$$

Here, taking into account that h = 1, k = 0 and l = 0 from reflection (200), the last term of expression (9) is equal to zero, and from this expression a is determined as follows;

$$a = d \cdot h, \tag{11}$$

and the lattice parameters are a_{Sn} = 0.5831 nm and c_{Sn} = 0.3412 nm, respectively. The unit cell of tin nanocrystallites has a body-centered tetragonal system corresponding to the space group $I4_1$/amd.

CONCLUSIONS

Thus, it was found that in the X-ray diffraction patterns of n-Si and Si<Sn> samples, structural reflections (110) of the corresponding SiO_2 nanocrystallites (quartz nanoinclusions) are observed at scattering angles of $2\theta \approx 36.6°$ with sizes of 14 nm and 17 nm in the boundary regions of the samples. It has been established that the lattice parameters of the unit cells of these nanoinclusions belonging to the hexagonal crystal lattice and space group $P3_21$ are a = b = 0.4936 nm and c = 0.5212 nm. It was found that the intensity of the main reflection (111) at a scattering angle of $2\theta = 28.63°$ with d/n = 0.3144 nm decreases by 23% and shifts toward larger angles ($\Delta\theta = 0.11^{o}$) due to a decrease in the parameters of the matrix crystal lattice samples of Si<Sn>, due to the interchangeability of silicon and tin atoms. It has been established that the sizes of tin nanocrystallites are 9.1 and 8 nm in the near-surface regions of the matrix lattice of Si<Sn> sample wafers. The unit cell of tin nanocrystallites has a tetragonal system with lattice parameters a_{Sn} = 0.5831 nm and c_{Sn} = 0.3412, corresponding to the space group $I4_1$/amd.

ORCID
Sharifa B. Utamuradova, https://orcid.org/0000-0002-1718-1122

REFERENCES

[1] B.S. Ahmed, B. Anissa, D. Radouan, N. Al Bouzieh, I.K. Durukan, and N. Amrane, East Eur. J. Phys. (1), 294 (2024), https://doi.org/10.26565/2312-4334-2024-1-26
[2] K.S. Daliev, S.B. Utamuradova, J.J. Khamdamov, and M.B. Bekmuratov, "Structural properties of silicon doped rare earth elements ytterbium," East European Journal of Physics, (1), 375–379 (2024). https://doi.org/10.26565/2312-4334-2024-1-37
[3] K.S. Daliev, S.B. Utamuradova, J.J. Khamdamov, and Z.E. Bahronkulov, "Electrophysical properties of silicon doped with lutetium," Advanced Physical Research, **6**(1), 42–49 (2024). https://doi.org/10.62476/apr61.49
[4] Kh.S. Daliev, and Z.M. Khusanov, East Eur. J. Phys. (1), 366 (2024), https://doi.org/10.26565/2312-4334-2024-1-35
[5] T.V. Kritskaya, V.N. Zhuravlev, and V.S. Berdnikov, "The ability to use an inert gas flow to control the qualitative characteristics of grown silicon single crystals," News from universities. Electronic materials, **22**(3), 158-167 (2019). https://doi.org/10.17073/1609-3577-2019-3-158-167
[6] Kh.S. Daliev, Z.E. Bahronkulov, and J.J. Hamdamov, East Eur. J. Phys. (4), 167 (2023), https://doi.org/10.26565/2312-4334-2023-4-18
[7] R.S. Madatov, A.S. Alekperov, F.N. Nurmammadova, N.A. Ismayilova, and S.H. Jabarov, East Eur. J. Phys. (1), 322 (2024), https://doi.org/10.26565/2312-4334-2024-1-29
[8] K.P. Abdurakhmanov, Kh.S. Daliev, Sh.B. Utamuradova, and N.Kh. Ochilova, "On defect formation in silicon with impurities of manganese and zinc," Applied Solar Energy (English translation of Geliotekhnika), **34**(2), 73–75 (1998). http://www.scopus.com/inward/record.url?eid=2-s2.0-77949325013&partnerID=MN8TOARS
[9] Z.T. Azamatov, M.A. Yuldoshev, N.N. Bazarbayev, and A.B. Bakhromov, "Investigation of Optical Characteristics of Photochromic Materials," Physics AUC, **33**, 139-145 (2023). https://cis01.central.ucv.ro/pauc/vol/2023_33/13_PAUC_2023_139_145.pdf
[10] V.N. Lozovsky, L.S. Lunin, and B.M. Seredin, "Features of silicon doping using the thermomigration method. News of higher educational institutions," Electronic materials, **18**(3), 179-188 (2015). https://doi.org/10.17073/1609-3577-2015-3-179-188
[11] K.A. Ismailov, Z.M. Saparniyazova, G.T. Kudeshova, G.A. Seytimbetova, and F.A. Saparov, East Eur. J. Phys. (1), 327 (2024), https://doi.org/10.26565/2312-4334-2024-1-30
[12] Sh.B. Utamuradova, Z.T. Azamatov, and M.A. Yuldoshev, Russian Microelectronics, **52**, Suppl. 1, S99-S103 (2023). https://doi.org/10.1134/S106373972360022X
[13] K.P. Abdurakhmanov, Sh.B. Utamuradova, Kh.S. Daliev, N.Kh. Ochilova, and Z.O. Olimbekov, "Study of the interimpurity interaction in silicon doped with platinum and iron," Applied Solar Energy (English translation of Geliotekhnika), **34**(2), 71–72 (1998).
[14] S.Z. Zainabidinov, Kh.S. Daliev, K.P. Abdurakhmanov, Sh.B. Utamuradova, I.Kh. Khomidjonov, and I.A. Mirzamurodov, "The influence of the impurities with deep levels on the iron behavior in silicon," Modern Physics Letters B, **11**(20), 909–912 (1997). http://dx.doi.org/10.1142/S0217984997001110
[15] K.V. Ravi, *Imperfections and impurities in semiconductor silicon*, (Wiley, New York, 1981). https://lib.ugent.be/catalog/rug01:001484099
[16] N.A. Hassan, W.H. Albanda, and M.H. Al-Timimi, East Eur. J. Phys. (3), 296 (2023), https://doi.org/10.26565/2312-4334-2023-3-28
[17] Z. He, X. Zhang, X. Wei, D. Luo, H. Ning, Q. Ye, R. Wu, et al., "Solution-Processed Silicon Doped Tin Oxide Thin Films and Thin-Film Transistors Based on Tetraethyl Orthosilicate," Membranes, **12**, 590 (2022). https://doi.org/10.3390/membranes12060590
[18] D. Comedi, O.H.Y. Zalloum, E.A. Irving, J. Wojcik, T. Roschuk, M.J. Flynn, and P. Mascher, "X-ray-diffraction study of crystalline Si nanocluster formation in annealed silicon-rich silicon oxides," Journal of Applied Physics, **99**(2), 023518 (2006). https://doi.org/10.1063/1.2162989
[19] D. Comedi, O.H.Y. Zalloum, E.A. Irving, J. Wojcik, T. Roschuk, M.J. Flynn, and P. Mascher, "X-ray-diffraction study of crystalline Si nanocluster formation in annealed silicon-rich silicon oxides," Journal of Applied Physics, **99**(2), 023518 (2006). https://doi.org/10.1063/1.2162989
[20] C.S.G. Cousins, L. Gerward, and J.S. Olsen, "Multiple diffraction in crystals studied by an X-ray energy-dispersive method," Physica status solidi (a), **48**(1), 113-119 (1978). https://doi.org/10.1002/pssa.2210480115
[21] Y.-H. Miao, H.-Y. Hu, J.-J. Song, R.-X. Xuan, and H.-M. Zhang, "Effects of rapid thermal annealing on crystallinity and Sn surface segregation of $Ge_{1-x}Sn_x$ films on Si (100) and Si (111)," Chinese Physics B, **26**(12), 127306 (2017). https://doi.org/10.1088/1674-1056/26/12/127306
[22] R.A. Puglisi, C. Vecchio, S. Lombardo, S. Lorenti, and M.C. Camalleri, "Charge transport in ultrathin silicon rich oxide/SiO_2 multilayers under solar light illumination and in dark conditions," Journal of Applied Physics, **108**(2), 023701 (2010). https://doi.org/10.1063/1.3463381
[23] I. Khidirov, editor, *Neutron diffraction*, (InTech, Rijeka, Croatia, 2012). http://www.intechopen.com/books/neutron-diffraction
[24] G. Will, *Powder Diffraction: The Riyetveld Method and the Two Stage Method of Determine and Refine Crystal Structures from Powder Diffraction Data*, (Springer, New York, 2005).

ОСОБЛИВОСТІ БУДОВИ КРЕМНІЮ З ДОМІШКАМИ ОЛОВА

Шаріфа Б. Утамурадова, Баходір Б. Бокієв,Ділором С. Пулатова
Інститут фізики напівпровідників і мікроелектроніки Національного університету Узбекистану, Ташкент, Узбекистан

У даній роботі методом рентгенівської дифракції та електронної мікроскопії досліджено зразки монокристалічного кремнію, легованого оловом. Встановлено, що при куті розсіювання $2\theta \approx 36.6°$ на дифрактограмах зразків n-Si та Si<Sn> спостерігаються структурні рефлекси (110) відповідних нанокристалітів SiO_2 з параметрами ґратки. a = b = 0,4936 нм і c = 0,5212 нм і c = 0,5212 нм, що належать до гексагональної кристалічної ґратки та просторової групи P321. Виявлено утворення нанокристалітів олова розміром 9,1 та 8 нм у приповерхневих областях кристалічної решітки матриці Si<Sn>.

Ключові слова: *кремній; олово; рентгенівська дифракція; субкристалітна кристалічна ґратка; нанокристалліт*